



HAL
open science

Radiation Induced by Charged Particles in Optical Fibers

X. Artru, C. Ray

► **To cite this version:**

X. Artru, C. Ray. Radiation Induced by Charged Particles in Optical Fibers. Moh. Yasin, Sulaiman W. Harun and Hamzah Arof. Selected Topics on Optical Fiber Technology, InTech (Open access Publisher) Vienna, pp.571-586, 2012. in2p3-00672964

HAL Id: in2p3-00672964

<https://in2p3.hal.science/in2p3-00672964>

Submitted on 22 Feb 2012

HAL is a multi-disciplinary open access archive for the deposit and dissemination of scientific research documents, whether they are published or not. The documents may come from teaching and research institutions in France or abroad, or from public or private research centers.

L'archive ouverte pluridisciplinaire **HAL**, est destinée au dépôt et à la diffusion de documents scientifiques de niveau recherche, publiés ou non, émanant des établissements d'enseignement et de recherche français ou étrangers, des laboratoires publics ou privés.

Radiation induced by charged particles in optical fibers

Xavier Artru and Cédric Ray
Université de Lyon, Université Lyon 1 and CNRS-IN2P3,
Institut de Physique Nucléaire de Lyon

[†] *Email: x.артру@ipnl.in2p3.fr*

1 Introduction

The electric field of a charged particle passing through or near an optical fiber induces a transient charges and currents in the fiber medium [1, 2]. These charges and current radiates electromagnetic waves, both outside the fiber (free light) and inside (guided light). This chapter is devoted to the guided light, which will be referred to as PIGL, for *Particle Induced Guided Light*.

If the fiber radius is large enough and the particle passes through it, as in Fig. 1, both PIGL and outside radiation can be considered as transition radiation and becomes Cherenkov radiation when the particle velocity exceeds that of light in the medium. This is the basis of the quartz fibre particle detectors [3, 4, 5]. Let us mention two other uses of optical fibers as particle detectors : (i) as dosimeters, through the effect of darkening by irradiation [6]; (ii) in scintillating glass fibers for particle tracking.

Here we will consider fibers of radius a comparable to the wavelength, in which case the standard OTR or Cherenkov descriptions are not appropriate. Two types of PIGL have to be considered :

- Type I : The particle passes *near* or *through* a straight or weakly bent part of the fibre, far from an extremity. Translation invariance along the fiber axis is essential.
- Type II : The particle passes near or through an end of the fiber or an added structure (e.g., metallic balls glued on the fibre surface), which is not translation invariant.

2 Particle-induced guided light of Type-I

The PIGL intensity will be calculated in the framework of quantized fields used by Glauber [7]. We will use relativistic quantum units familiar to particle physicists : $\hbar = c = \varepsilon_0 = \mu_0 = 1$. $\lambda \equiv \lambda/2\pi = 1/\omega$. The Gauss law is written $\nabla \cdot \mathbf{E} = \rho$, not $4\pi\rho$. $e^2/(4\pi) = \alpha = 1/137$.

2.1 Expansion of the field in proper modes

The fiber is along the $\hat{\mathbf{z}}$ axis. The cylindrical coordinates are (r, ϕ, z) . $\mathbf{r} = (x, y)$ is the transverse position. $x \pm iy = re^{\pm i\phi}$.

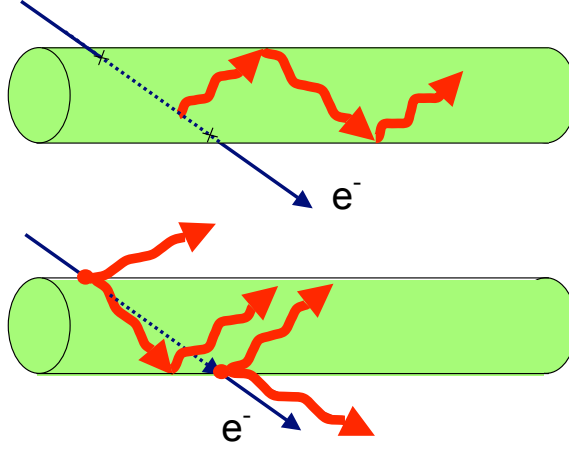


Figure 1: Standard mechanisms of production of light inside a fiber, by an electron passing through. Top: Cherenkov radiation. Bottom: Transition radiation.

The quantized electromagnetic field \mathbf{E}^{op} in presence of the fiber can be expanded in propagation modes :

$$\mathbf{E}^{op}(t, \mathbf{X}) = \int_0^\infty \frac{d\omega}{2\pi} \sum_m a_m(\omega) \vec{\mathcal{E}}^{(m)}(\omega; \mathbf{X}) \exp(-i\omega t) + \text{hermit. conj.} \quad (1)$$

The complex-valued field

$$\vec{\mathcal{E}}^{(m)}(\omega; \mathbf{X}) = \mathbf{E}^{(m)}(\omega; \mathbf{r}) \exp(ipz) \quad (2)$$

is a “photon wave function”. $m = \{M, \nu, \sigma\}$ is a collective index which gathers the total angular momentum $M \equiv J_z = L_z + S_z$ of the photon, the radial quantum number ν and the direction of propagation $\sigma = \text{sign}(p) = \pm 1$. a_m and a_m^\dagger are the destruction and creation operators of a photon in the mode m . ω and p are linked by the dispersion relation,

$$\omega = \omega_m(p) \quad \text{or} \quad p = p_m(\omega). \quad (3)$$

The ν spectrum has a discrete part for guided modes and a continuous part for free modes. The summation over m in (1) implies that ν is treated as a fully discrete variable, for simplicity. This is actually the case if we quantize the field inside a cylindrical box.

The quantized magnetic field is expanded like in (1). a_m and a_m^\dagger obey the commutation rules

$$\left[a_{M,\nu,\sigma}(\omega), a_{M',\nu',\sigma'}^\dagger(\omega') \right] = 2\pi \delta(\omega - \omega') \delta_{MM'} \delta_{\nu\nu'} \delta_{\sigma\sigma'}. \quad (4)$$

For a fixed ω the modes m are orthonormal in the sense

$$\int d^2\mathbf{r} \left[\mathbf{E}^{(m)*}(\omega; \mathbf{r}) \times \mathbf{B}^{(n)}(\omega; \mathbf{r}) + \mathbf{E}^{(n)}(\omega; \mathbf{r}) \times \mathbf{B}^{(m)*}(\omega; \mathbf{r}) \right]_z = \omega \delta_{mn}. \quad (5)$$

For $n = m$, the left-hand side is the power carried by the fiber in the mode m , which is $\hbar\omega$ (= one photon) per unit of time.

Equations (1), (4) and (5) correspond to Eqs. (2.29b), (2.25b) and (2.14a) of Ref.[7]. The correspondance would be $\mathbf{f}_\mathbf{k} \rightarrow -i(2/\omega)^{1/2} \mathbf{E}^{(m)}$, but we use the continuous variable ω instead of a fully discrete set of quantum numbers. a_m and $\mathbf{E}^{(m)}$ differ from those of Ref.[1] by a factor $(dp/d\omega)^{1/2} = v_g^{-1/2}$. The factor 2 in (5) was forgotten in Refs.[1, 2], leading to an overestimation of the photon production yield by a factor 2.

2.2 Wave functions of the fiber modes

The propagation modes in optical fibers can be found in several textbooks, e.g. [8]. Nevertheless, it is useful to present a short review based on states of definite angular momentum M .

We assume that the fiber has an homogeneous refractive index $n = \sqrt{\varepsilon}$ and no clad. For a guided mode the phase velocity $v_{\text{ph}} = \omega/p$ is in the interval $[1/n, 1]$. The photon transverse momentum is $q = \sqrt{\varepsilon\omega^2 - p^2}$ inside the fiber and $i\kappa = i\sqrt{p^2 - \omega^2}$ (evanescent wave) outside the fiber. The longitudinal parts of the fields have $S_z = 0$ therefore their orbital angular momentum L_z is equal to M . Using cylindrical coordinates (r, ϕ, z) they write

$$E_z(\mathbf{r}) = i e^{iM\phi} f_z(r), \quad B_z(\mathbf{r}) = e^{iM\phi} h_z(r), \quad (6)$$

Both in medium and in vacuum f_z and h_z obey the same differential equation

$$[\partial_r^2 + r^{-1}\partial_r - M^2/r^2 + k_T^2(r)] f_z \text{ or } h_z = 0 \quad (\text{except for } r = a) \quad (7)$$

where $k_T^2(r) = q^2$ inside the fiber and $k_T^2(r) = -\kappa^2$ outside the fiber.

The piecewise solutions of (7) are Bessel functions J_M or K_M . From the fact that f_z and h_z are continuous at $r = 0$ and $r = a$ and decreasing at $r \rightarrow \infty$, it follows that $h_z(r)/f_z(r)$ is independent on r . We write

$$f_z(r) = c_E \psi(r), \quad h_z(r) = c_B \psi(r), \quad (8)$$

$$\psi(r) = J_M(qr) \text{ inside, } \psi(r) = c_K K_M(\kappa r) \text{ outside, } c_K = \frac{J_M(qa)}{K_M(\kappa a)}.$$

The transverse components \mathbf{E}_T and \mathbf{B}_T can be expressed either in terms of the radial and azimuthal basic vectors, $\hat{\mathbf{e}}^r = \mathbf{r}/r$ and $\hat{\mathbf{e}}^\phi = \hat{\mathbf{z}} \times \hat{\mathbf{e}}^r$,

$$\begin{aligned} \mathbf{E}_T &= e^{iM\phi} (f_r(r) \hat{\mathbf{e}}^r + f_\phi(r) \hat{\mathbf{e}}^\phi) \\ \mathbf{B}_T &= e^{iM\phi} (h_r(r) \hat{\mathbf{e}}^r + h_\phi(r) \hat{\mathbf{e}}^\phi), \end{aligned} \quad (9)$$

or in terms of the $S_z = \pm 1$ eigenvectors $\hat{\mathbf{e}}^\pm = (\hat{\mathbf{x}} \pm i\hat{\mathbf{y}})/2$:

$$\begin{aligned}\mathbf{E}_T &= e^{i(M-1)\phi} f_-(r) \hat{\mathbf{e}}^+ + e^{i(M+1)\phi} f_+(r) \hat{\mathbf{e}}^- \\ i\mathbf{B}_T &= e^{i(M-1)\phi} h_-(r) \hat{\mathbf{e}}^+ + e^{i(M+1)\phi} h_+(r) \hat{\mathbf{e}}^-\end{aligned}\quad (10)$$

with $f_\pm = f_r \pm if_\phi$ and $-ih_\pm = h_r \pm ih_\phi$. The $\hat{\mathbf{e}}^+$ and $\hat{\mathbf{e}}^-$ parts of the fields have orbital momenta $L_z = M \mp 1$, therefore their radial dependence are Bessel functions of order $M \mp 1$:

$$\begin{aligned}f_\pm(r) &= c_{fJ}^\pm J_{M\pm 1}(qr) \quad (r \leq a), & c_{fK}^\pm K_{M\pm 1}(\kappa r) \quad (r > a), \\ h_\pm(r) &= c_{hJ}^\pm J_{M\pm 1}(qr) \quad (r \leq a), & c_{hK}^\pm K_{M\pm 1}(\kappa r) \quad (r > a).\end{aligned}\quad (11)$$

The Maxwell equations relate the transverse fields to the longitudinal ones. The formula in the $\{\hat{\mathbf{e}}^r, \hat{\mathbf{e}}^\phi\}$ basis can be found in [8]. Translated in the $\{\hat{\mathbf{e}}^+, \hat{\mathbf{e}}^-\}$ basis they give

$$\begin{aligned}c_{fJ}^\pm &= (\pm p c_E - \omega c_B)/q, & c_{fK}^\pm &= \mp(q c_K/\kappa) c_{fJ}^\pm, \\ c_{hJ}^\pm &= (\pm p c_B - \omega \varepsilon c_E)/q, & c_{hK}^\pm &= (-p c_B \pm \omega c_E) c_K/\kappa.\end{aligned}$$

The continuity of $h_z, h_r, h_\phi, f_z, f_\phi$ and $\epsilon(r)f_r$ at $r = a$ leads to

$$\frac{c_B}{c_E} = -MQ \left[\frac{J'_M(u)}{uJ_M(u)} + \frac{K'_M(w)}{wK_M(w)} \right]^{-1} = -\frac{1}{MQ} \left[\frac{\varepsilon J'_M(u)}{uJ_M(u)} + \frac{K'_M(w)}{wK_M(w)} \right] \quad (12)$$

where $u \equiv qa$, $w \equiv \kappa a$ and

$$Q = (u^{-2} + w^{-2})p/\omega = (\varepsilon u^{-2} + w^{-2})\omega/p.$$

From the two expressions of c_B/c_E in (12) one obtains

$$\left[\frac{J'_M(u)}{uJ_M(u)} + \frac{K'_M(w)}{wK_M(w)} \right] \cdot \left[\frac{\varepsilon J'_M(u)}{uJ_M(u)} + \frac{K'_M(w)}{wK_M(w)} \right] = M^2 \left(\frac{1}{u^2} + \frac{1}{w^2} \right) \cdot \left(\frac{\varepsilon}{u^2} + \frac{1}{w^2} \right), \quad (13)$$

which, together with $u^2 = (\varepsilon\omega^2 - p^2)a^2$ and $w^2 = (p^2 - \omega^2)a^2$, determines the dispersion relation (3).

2.2.1 Normalization of the mode wave functions

The z -component of the Pointing vector of the complex field is

$$\mathcal{P}^{(m)}(\mathbf{r}) = 2 \operatorname{Re} \left\{ \mathbf{E}^{(m)*} \times \mathbf{B}^{(m)} \right\}_z = \operatorname{Re} \left\{ f_-^*(r) h_-(r) - f_+^*(r) h_+(r) \right\}.$$

Using (11) and integrating over \mathbf{r} gives the mode power

$$\begin{aligned}P^{(m)} &= P_{\text{int}}^{(m)} + P_{\text{ext}}^{(m)} = \int_0^a 2\pi r dr \left\{ c_{fJ}^- c_{hJ}^- J_{M-1}^2(qr) - c_{fJ}^+ c_{hJ}^+ J_{M+1}^2(qr) \right\} \\ &\quad + \int_a^\infty 2\pi r dr \left\{ c_{fK}^- c_{hK}^- K_{M-1}^2(\kappa r) - c_{fK}^+ c_{hK}^+ K_{M+1}^2(\kappa r) \right\}.\end{aligned}\quad (14)$$

The coefficient c_E has to be adjusted to get the normalization (5).

Fig. 2 shows the phase velocity $v_{\text{ph}} = \omega/p$ of the lowest mode ($M = \pm 1, \nu = 1$) called HE_{11} and the external fraction of the mode power, as a function of ω . The index of refraction is $n = 1.41$ (fused silica).

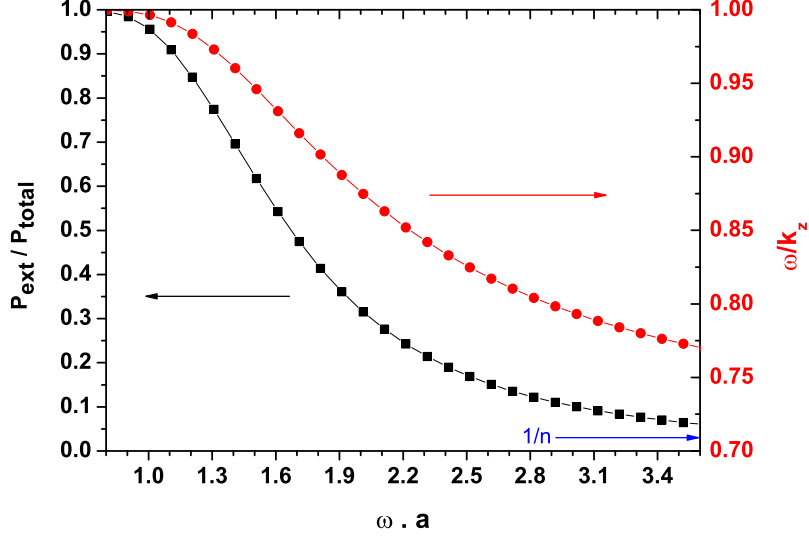


Figure 2: phase velocity $v_{\text{ph}} = \omega/p$ (balls, right scale) and external fraction of the power (squares, left scale) for the HE_{11} mode.

2.2.2 Linearly polarized modes

When changing M into $-M$, the above defined field modes change as follows :

$$\begin{aligned} \{\mathbf{E}_T, E_z, \mathbf{B}_T, B_z\}^{(-M)} &= (-1)^M \Pi(0^\circ) \{\mathbf{E}_T, E_z, \mathbf{B}_T, B_z\}^{(M)} \\ &= \Pi(90^\circ) \{\mathbf{E}_T, E_z, \mathbf{B}_T, B_z\}^{(M)} \\ &= (-1)^M \{\mathbf{E}_T^*, -E_z^*, \mathbf{B}_T^*, -B_z^*\}^{(M)}. \end{aligned} \quad (15)$$

$\Pi(\alpha)$ is the operator of mirror reflection about the plane $\phi = \alpha$, for instance

$$\Pi(0^\circ)\{E_x, E_y, E_z\}(x, y, z) = \{E_x, -E_y, E_z\}(x, -y, z)$$

and a similar formula for \mathbf{B} , with an extra $(-)$ sign since it is a pseudovector. The linear combination

$$\{\mathbf{E}, \mathbf{B}\}^{(M, 0^\circ)} = \left[\{\mathbf{E}, \mathbf{B}\}^{(M)} + (-1)^M \{\mathbf{E}, \mathbf{B}\}^{(-M)} \right] / \sqrt{2} \quad (16)$$

is even under $\Pi(0^\circ)$ and has real \mathbf{E}_T . For $M = 1$,

$$\mathbf{E}_T^{(1, 0^\circ)} = [f_-(r) \hat{\mathbf{x}} + f_+(r) (\cos 2\phi \hat{\mathbf{x}} + \sin 2\phi \hat{\mathbf{y}})] / \sqrt{2} \quad (17)$$

is the state whose dominant (f_-) part is linearly polarized parallel to $\hat{\mathbf{x}}$.

2.3 Bent fiber

Bending the fiber has several effects :

- a) small break-down of the degeneracy (*i.e.*, slightly different dispersion relations) between the polarized states $(M, 0^\circ)$ and $(M, 90^\circ)$, where 0° is the azimuth of the bending plane),
- b) co-rotation of the transverse wave function $\vec{\mathcal{E}}^{(m)}(\omega; \mathbf{X})$ with the unit vector $\hat{\mathbf{s}}$ tangent to the local fiber axis.
- c) escape of light by tunneling through a centrifugal barrier.

For large enough bending radius, effects a) and c) can be ignored. Effect b) is non-trivial when the bending is skew (not planar). Instead of (2), we have

$$\vec{\mathcal{E}}^{(m)}(\omega; \mathbf{X}) = \mathcal{R}_f(s) \mathbf{E}^{(m)}(\omega; \mathcal{R}_f^{-1}(s) \mathbf{r}) \exp(i\mathbf{p}s), \quad (18)$$

where $\mathbf{X}_f(s)$ is the point of the fiber axis nearest to \mathbf{X} , s its curvilinear abscissa and $\mathbf{r} = \mathbf{X} - \mathbf{X}_f(s)$ (see Fig. 3 left). $\mathcal{R}_f(s)$ is a finite rotation matrix resulting from a succession of infinitesimal rotations $\mathcal{R}(\hat{\mathbf{s}} \rightarrow \hat{\mathbf{s}} + d\hat{\mathbf{s}})$:

$$\mathcal{R}_f(s + ds) = \mathcal{R}(\hat{\mathbf{s}} \rightarrow \hat{\mathbf{s}} + d\hat{\mathbf{s}}) \circ \mathcal{R}_f(s), \quad \mathcal{R}_f(0) = \mathbf{I}, \quad (19)$$

$\mathcal{R}(\hat{\mathbf{s}} \rightarrow \hat{\mathbf{s}}')$ denoting the rotation along $\hat{\mathbf{s}} \times \hat{\mathbf{s}}'$ which transforms $\hat{\mathbf{s}}$ into $\hat{\mathbf{s}}'$. Taking into account the non-commutativity of the rotations, we have

$$\mathcal{R}_f(s) = \mathcal{R}(\hat{\mathbf{s}}, \Omega(s)) \circ \mathcal{R}(\hat{\mathbf{z}} \rightarrow \hat{\mathbf{s}}). \quad (20)$$

where $\hat{\mathbf{z}}$ is the orientation of the beginning of the fiber, $\mathcal{R}(\hat{\mathbf{s}}, \alpha)$ stands for a rotation of angle α about $\hat{\mathbf{s}}$ and $\Omega(s)$ is the dark area on the unit sphere in Fig. 3 (right). For a state of given angular momentum M in (18) one can replace $\mathcal{R}_f(s)$ by $\mathcal{R}(\hat{\mathbf{z}} \rightarrow \hat{\mathbf{s}})$ and take into account the first factor of (20) by the *Berry phase* factor $\exp[-iM\Omega(s)]$. If the fiber is bent in a plane, $\Omega(s) = 0$.

2.4 Mode excitation by a charged particle

When a particle of charge Ze passes *trough* or *near* the fiber, it can create one or several photons by spontaneous or stimulated emission. Neglecting its loss of energy and momentum, the particle acts like a classical current and the excitation of the quantum field is a *coherent state* [7]. The spontaneous photon emission amplitude in the mode m , corresponding to Eqs. (7.11) and (7.16) of [7], is

$$R^{(m)}(\omega) = \frac{Ze}{\omega} \int d\mathbf{X}(t) \cdot \vec{\mathcal{E}}^{(m)*}(\omega; \mathbf{X}) \exp(i\omega t) \quad (21)$$

for a mode normalized according to (5). The photon spectrum of spontaneous emission in the mode m reads

$$\frac{d\mathcal{N}_{\text{phot}}^{(m)}}{d\omega} = \frac{\omega}{2\pi P^{(m)}(\omega)} \left| R^{(m)}(\omega) \right|^2. \quad (22)$$

Thanks to the factor $P^{(m)}(\omega)$ given by (14) in the denominator, this expression is invariant under a change of the normalisation of the mode fields.

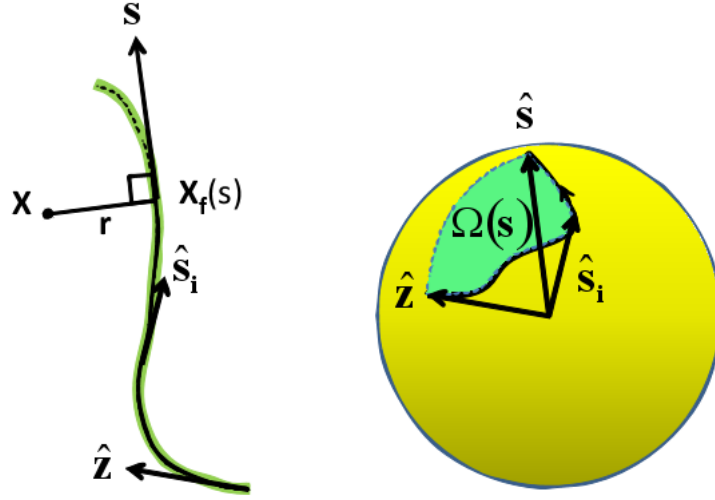


Figure 3: Left: bent fiber and definition of $\mathbf{X}_f(s)$ and \mathbf{r} . Right: curve drawn by the extremities of successive tangent vectors ($\hat{\mathbf{z}}, \hat{\mathbf{s}}_i, \hat{\mathbf{s}}, \dots$) on the unit sphere and definition of the solid angle $\Omega(s)$. The dotted arc of circle represents the “most direct” rotation, $\mathcal{R}(\hat{\mathbf{z}} \rightarrow \hat{\mathbf{s}})$, transforming $\hat{\mathbf{z}}$ into $\hat{\mathbf{s}}$.

2.5 Straight fiber and particle in rectilinear uniform motion

For a particle following the straight trajectory

$$\mathbf{X} = \mathbf{b} + \mathbf{v}t, \quad \mathbf{b} = (b, 0, 0), \quad \mathbf{v} = (0, v_T, v_L), \quad (23)$$

Eqs.(21) and (2) give

$$R^{(m)}(\omega) = \frac{Ze}{\omega} \int_{-\infty}^{\infty} dy \left[E_y^{(m)}(x, y) + \frac{v_L}{v_T} E_z^{(m)}(x, y) \right]^* \exp\left(iy \frac{\omega - v_L p}{v_T} \right) \quad (24)$$

Using (6-11) one arrives at the pure imaginary expression

$$R^{(m)}(\omega) = \frac{-iZe}{\omega} \int_0^{\infty} dy \{ \cos[\eta y + (M-1)\phi] f_-(r) - \cos[\eta y + (M+1)\phi] f_+(r) + 2(v_L/v_T) \cos(\eta y + M\phi) f_z(r) \} \quad (25)$$

with $r = \sqrt{b^2 + y^2}$, $\phi = \tan^{-1}(y/b)$ and

$$\eta = (v_L p - \omega)/v_T = (v_L - v_{ph}) p/v_T.$$

The energy of the light pulse is obtained by multiplying by ω_C . This formula applies in particular to the limit of small crossing angles considered above. The photon number increases linearly with the path length over which the particle travels inside or close to the fiber.

2.8 Numerical results for straight electron trajectory and straight fiber

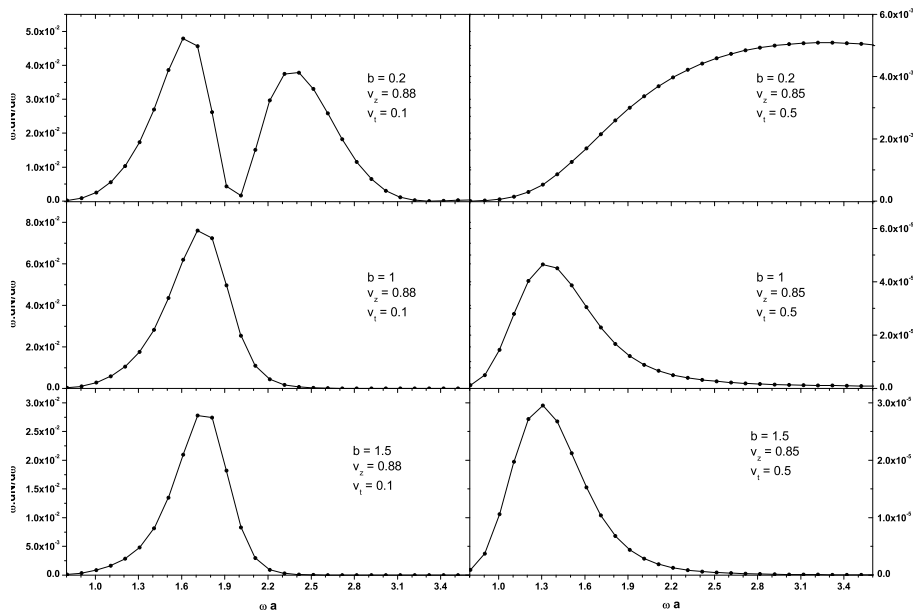


Figure 4: Dimensionless photon spectrum $\omega d\mathcal{N}_{\text{phot}}/d\omega$ as a function of ωa in the HE_{11} mode for six types of the particle trajectory and $M = +1 = \text{sign}(v_T)$.

The dimensionless photon spectrum $\omega d\mathcal{N}_{\text{phot}}/d\omega$ in the fundamental mode HE_{11} of a fused silica fiber is plotted in Fig. 4 for three impact parameters, $b = 0.2a$ (penetrating trajectory), $b = a$ (tangent trajectory) and $b = 1.5a$ (fully external trajectory), and two particle velocity vectors, $(v_L, v_T) = (0.88, 0.1)$ and $(v_L, v_T) = (0.85, 0.5)$, corresponding to large and moderate angle respectively. We took the sign of M to be the same as the J_z of the particle.

The spectra are harder for penetrating trajectories, due to (i) the discontinuity of the fields at the fiber surface, (ii) the lower importance of the evanescent field at high frequency.

In the large angle - penetrating case, the dimensionless yield is of the order of $\alpha = e^2/(4\pi) = 1/137$. In the tangent case it is much smaller. Note the peak at a relatively small frequency, where the wave travels mainly outside the fiber (see Fig. 2). At still smaller frequency, the wave function of the mode

becomes too much diluted, which explains the vanishing yields at small ω in the six curves.

In the $b = 0.2a$ and $v_T = 0.1$ case, we have a dip at $\omega a = 2$ instead of an expected Cherenkov peak fixed by Eq.(26). This is a peculiarity of the odd M modes when b is small : if $b = 0$, then ϕ in (25) is either $-\pi/2$ or $+\pi/2$ and, at the Cherenkov point ($\eta = 0$), $\cos(\eta y + M\phi)$ is zero in the whole integration range.

A separate figure (Fig. 5) at small crossing angle ($v_T/v_L = 0.03/0.95$) shows the narrow peak of “fiber Cherenkov light” at the position $\omega a \simeq 1.4$ predicted by (26) and Fig. 2. The half-width at half maximum, 0.06, corresponds roughly to the condition $|v_L - v_{\text{ph}}| \lesssim v_T/(pa)$ mentioned in Paragraph 2.6.

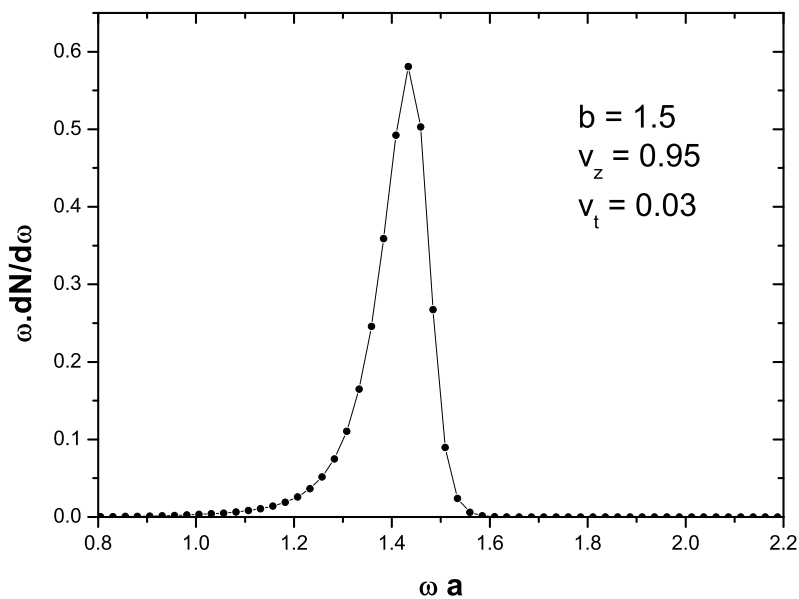


Figure 5: Photon yields in the HE_{11} mode with $M = +1$ for a small crossing angle : $(v_L, v_T) = (0.95, 0.03)$; $b = 1.5a$.

2.9 Polarisation

If $b = 0$, the HE_{11} guided light is linearly polarized in the particle incidence plane. If $b \neq 0$, some circular polarization is expected. One could naively expect that the favored photon angular momentum M has the sign of the azimuthal speed of the particle, i.e. the sign of v_T in (23), but this is not always true. What matters in fact is not the sign of M but the sense of rotation of the electric field of the mode in the *moving plane* $z = vt$. In this plane the azimuth of the field varies like $M(\omega t - pz) = (v_{\text{ph}} - v_L) M\omega t/v_{\text{ph}}$. If the moving plane is faster than the wave, the field rotates in the opposite way. Thus the favored sign of

M is the sign of $(v_{\text{ph}} - v_L) v_T$. This can be seen from (25) : if M and η have the same sign, the integrand oscillate faster and the amplitude is reduced.

In Figs. 4 and 5, M has the sign of v_T . This circular polarization is favored at $v_{\text{ph}} > v_L$, whence $\omega < \omega_C(v_L)$, and unfavored at $v_{\text{ph}} < v_L$, whence $\omega > \omega_C(v_L)$. This partly explains the asymmetric shape of the fiber Cherenkov peak in Fig. 5. Changing the sign either of M or of v_T should result in a harder spectrum.

2.10 Interferences with periodically bent trajectory or bent fiber

With an undulated trajectory, as in Fig. 6a or an undulated fiber as in Fig. 6b, one can have several meeting points, the PIGL amplitude of which, given by (25) or (28), add coherently. Let L_f and L_p be the lengths of the fiber and of the particle trajectory between two meeting points. Two successive fiber-particle interactions are separated in time by $\Delta t = L_f/v$ and their phase difference is

$$\Delta\Phi = p L_f - \omega \Delta t = \omega (L_f/v_{\text{ph}} - L_p/v) . \quad (33)$$

If N equivalent meeting points are spaced periodically, the frequency spectrum is

$$\left(\frac{d\mathcal{N}^{(m)}}{d\omega} \right)_{N \text{ meeting}} = \left(\frac{d\mathcal{N}^{(m)}}{d\omega} \right)_{1 \text{ meeting}} \times \frac{\sin^2(N\Delta\Phi/2)}{\sin^2(\Delta\Phi/2)} . \quad (34)$$

The last fraction is the usual interference factor in periodical systems, e.g. in undulator radiation. For large N it gathers the photon spectrum in quasi-monochromatic lines fixed by

$$\omega (L_f/v_{\text{ph}} - L_p/v) = 2k\pi \quad (k \text{ integer}) . \quad (35)$$

If the fiber bending is *not planar*, but for instance helicoidal (Fig. 6c), the left- and right circular polarisations have different phase velocities. Their propagation amplitudes acquire an additional phase $\phi_B = -M\Omega$, called the *Berry phase*, where Ω is the solid angle of the cone drawn by the local axis of the fiber [11] (as if $\hat{\mathbf{s}}$ coincides with $\hat{\mathbf{z}}$ in Fig. 3). The preceding condition becomes

$$\omega (L_f/v_{\text{ph}} - L_p/v) = 2k\pi - \phi_B . \quad (36)$$

The interferences disappear when the velocity spread of the charged particle beam is such that the variation of $\omega L_p/v$ is more than, say, 2π .

2.11 Application of type-I PIGL to beam diagnostics

PIGL in a monomode fiber is intense enough not for single particle detection, but for beam diagnostics.

The ‘‘fiber Cherenkov radiation’’ can be used to measure the velocity of a semi-relativistic particle beam, using the dependence of v_{ph} on ω shown in Fig. 2.

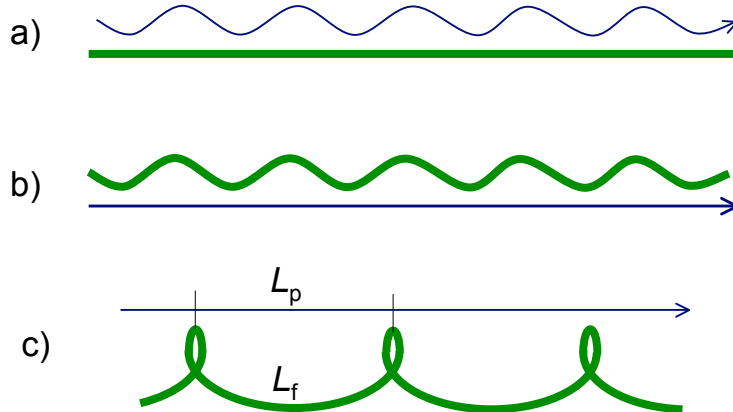


Figure 6: periodically bent particle trajectory (a), planar bent fiber (b) and helical bent fiber (c). L_p and L_f are the lengths of the curved or straight periods, for the particle and the fiber respectively.

In a periodically bent fiber, the interference can test the velocity spread of the beam.

At large crossing angle, a fiber can measure the transverse profile of the beam with a resolution of the order of the diameter $2a$. No background is made by real photons coming from distant sources (for instance synchrotron radiation from upstream bending magnets). Indeed, such photons are in the continuum spectrum of the radial number ν , therefore they are not captured by the fiber, but only scattered. This is an advantage over beam diagnostic tools like optical transition radiation (OTR) and optical diffraction radiation (ODR). The translation invariance along the fiber axis, which guarantees the conservation of ν , is essential for this property.

The resolution power of PIGL is also not degraded by the large transverse size $\sim \gamma\lambda$ of the virtual photon cloud at high Lorentz factor $\gamma = (1 - v^2)^{-1/2}$. Indeed, the virtual photons at transverse distance $\gg \lambda$ are almost real, therefore are not captured by the fiber.

3 Particle-induced guided light of Type-II

The second type of PIGL is produced at a place where the fiber is not translation invariant. We consider two examples : 1) PIGL from the cross section of a cut fiber, 2) PIGL assisted by metallic balls glued to the fiber. These devices are represented in Fig. 7.

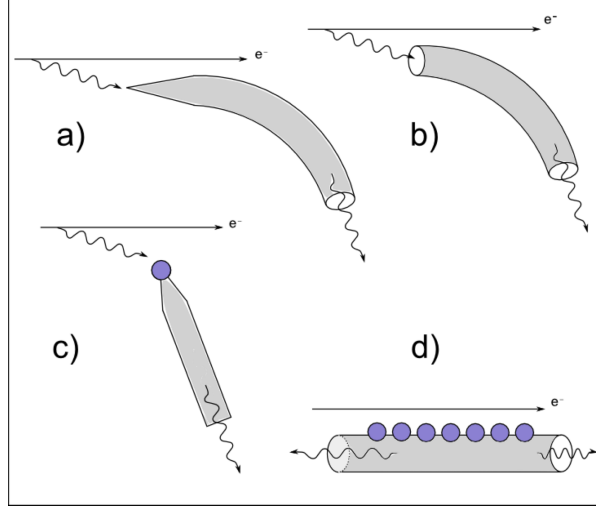


Figure 7: Part of fiber which can capture virtual photons for Type-II PIGL : a) conical end ; b) sharp-cut end ; c) metallic ball glued on one end ; d) regularly spaced metallic balls glued along the fiber.

3.1 PIGL from the cross section of a cut fiber

The entrance section of a sharp-cut fiber can catch free real photons and convert them into guided photons. Assuming that the photons are incident at small angle with the fiber axis, the energy spectrum captured by the fiber in the mode $m = \{M, \nu\}$ is given by

$$\frac{dW^{(m)}}{d\omega} = \frac{1}{2\pi P^{(m)}(\omega)} \times \left| \int d^2\mathbf{r} \left[T_B(\mathbf{r}) \mathbf{E}_T^{(m)*}(\omega; \mathbf{r}) \times \mathbf{B}_T^{\text{in}}(\omega; \mathbf{r}) + T_E(\mathbf{r}) \mathbf{E}_T^{\text{in}}(\omega; \mathbf{r}) \times \mathbf{B}_T^{(m)*}(\omega; \mathbf{r}) \right] \right|^2. \quad (37)$$

where $\{\mathbf{E}^{\text{in}}, \mathbf{B}^{\text{in}}\}$ is the incoming field on the cutting plane. $T_E(\mathbf{r})$, $T_B(\mathbf{r})$ are the Fresnel refraction coefficients at normal incidence, given by

$$T_E(\mathbf{r}) = 2/(1 + \sqrt{\varepsilon(\mathbf{r})}), \quad T_B(\mathbf{r}) = \sqrt{\varepsilon(\mathbf{r})} T_E(\mathbf{r}). \quad (38)$$

$\varepsilon(\mathbf{r})$ is the local permittivity of the fiber. Outside the fiber, $T_E(\mathbf{r}) = T_B(\mathbf{r}) = 1$. Equation (37) is deduced from the orthonormalization relation (5).

With some caution (37) can be applied to the capture of virtual photons from the Coulomb field of a relativistic particle passing near the entrance face (see Fig. 7b). The transverse component of this field is given by [12, 13]

$$\mathbf{E}_T^{\text{in}}(\omega; \mathbf{r}) = \frac{Ze\omega}{2\pi\gamma v^2 b} K_1\left(\frac{\omega b}{\gamma v}\right) \mathbf{b}, \quad \mathbf{B}_T^{\text{in}}(\omega; \mathbf{r}) = \mathbf{v} \times \mathbf{E}_T^{\text{in}}(\omega; \mathbf{r}). \quad (39)$$

Here $\mathbf{b} = \mathbf{r} - \mathbf{r}_{\text{particle}}$ is the impact parameter relative to the particle. It must be large enough compared to λ , otherwise the incoming photon is too different from a real one.

3.2 PIGL from a conical end of fiber

The sharp-cut fiber has a wide angular acceptance but is not optimized for capturing the virtual photon cloud accompanying an ultrarelativistic particle, which has an angular divergence $\sim 1/\gamma$. A more efficient capture is possible with a narrow conical end (Fig. 7a), at the price of a smaller acceptance. The wave function of a parallel photon may be quasi-adiabatically transformed into a guided mode without too much loss. This should be true for the photons of the Coulomb field in the impact parameter range $\lambda \ll b \lesssim \gamma\lambda$, which are quasi-real and have a small transverse momentum $k_T \sim 1/b$.

3.3 PIGL from metallic balls

It is also possible to capture a virtual photon with a metallic ball glued to the fiber, either at the extremity (Fig. 7c) [14, 15], or on the side as in Fig. 7d. Then a plasmon is created [16, 18], which has some probability p_f to be evacuated as guided light in the fiber.

A rough estimate of the capture efficiency can be obtained when the impact parameter of the particle is large compared to the ball radius R and the time scale $\Delta t \sim b/(\gamma v)$ of the transient field is short compared to the reduced period $1/\omega = \lambda$ of the plasmon: the particle field boosts each electron of the ball with a momentum $\mathbf{q} \simeq 2Z\alpha \mathbf{b}/(vb^2)$. It results in a collective dipole excitation of the electron cloud, of energy

$$W(b) \simeq \frac{4\pi R^3 n_e}{3} \left(\frac{2Z\alpha}{vb} \right)^2 \frac{1}{2m_e} = \frac{2Z^2\alpha}{3v^2} \frac{\omega_P^2 R^3}{b^2} \quad (R \ll b \ll \gamma v \lambda), \quad (40)$$

where $\omega_P = (4\pi\alpha n_e/m_e)^{1/2}$ is the plasma frequency of the infinite medium. For a spherical ball the dipole plasmon frequency is simply given by $\omega = \omega_P/\sqrt{3}$, assuming the Drude formula $\varepsilon = 1 - \omega_P^2/\omega^2$ and neglecting the retardation effects (case $R \lesssim \lambda$). The number of stored quanta is then

$$\mathcal{N}(b) = \frac{W(b)}{\omega} \simeq \frac{2Z^2\alpha}{v^2} \cdot \frac{R^3}{\lambda b^2}. \quad (41)$$

Taking $b_{\min} = R$ and $b_{\max} = \gamma v \lambda$, the cross section for this process is

$$\sigma = \int_{b_{\min}}^{b_{\max}} 2\pi b db \mathcal{N}(b) \simeq \frac{4Z^2\alpha}{v^2} \cdot \frac{R^3}{\lambda} \cdot \ln \frac{\gamma v \lambda}{R}. \quad (42)$$

More precise values of the plasmon frequencies are used in [16, 17, 18] in the context of Smith-Purcell radiation. Retardation effects and other multipoles are taken into account in [17, 18]. A typical order of the cross section, $\sigma \sim 10^{-2}\lambda^2$

is obtained with $R \sim \lambda$, $Z = 1$, $\gamma v \sim 1$. The plasmon wavelength is typically $\lambda \sim 10^2$ nm. Larger cross section can be realized by increasing R , but higher multipoles will dominate, unless γ is increased simultaneously. Discussions and experimental results about this point are given in [18].

The efficiency of the ball scheme depends on the ball-to-fiber transmission probability p_f , which is less than unity because the plasmon may also be radiated in vacuum or decay by absorption in the metal.

3.3.1 Interferences between several balls

If several metallic balls are glued at equal spacing l on one side of the fiber (Fig. 7d), constructive interferences (resonance peaks) are obtained when

$$\omega/v \mp p \equiv (1/v \mp 1/v_{\text{ph}})\omega = 2k\pi/l \quad (k \text{ integer}), \quad (43)$$

ω and p being linked by (3). The $-$ and $+$ signs correspond respectively to lights propagating forward and backward in the fiber. The forward light has the highest frequency. This process is in competition with the Smith-Purcell radiation from the balls, where $\mp 1/v_{\text{ph}}$ is replaced by $-\cos\theta_{\text{rad}}$. We can call it “guided Smith-Purcell” radiation. It is advantageous to choose l such that ω lies on a plasmon resonance of the ball.

3.3.2 Shadowing

The guided Smith-Purcell spectrum for N balls can be written as

$$\left(\frac{d\mathcal{N}^{(m)}}{d\omega}\right)_{N \text{ balls}} \simeq \left(\frac{d\mathcal{N}^{(m)}}{d\omega}\right)_{1 \text{ ball}} \times \frac{\sin^2(N\Delta\Phi/2)}{\sin^2(\Delta\Phi/2)} \times \text{shadow factor}. \quad (44)$$

This is similar to (34) except for a *shadow factor* which is less than unity. Indeed, each ball intercepts part of the virtual photon flux, thus makes a shadow on the following balls. The shadow of one ball has a longitudinal extension $l_f \sim v\lambda/(1-v) \sim \gamma^2 v\lambda$. Beyond this region, called *formation zone*, the cloud of virtual photons of wavelength λ is practically restored if there is no other piece of matter in the formation zone.

The shadow effect has been directly observed in diffraction radiation [19]. In the case of metallic balls it is included in the rescattering effects studied by García et al [20].

3.4 Application of Type-II PIGL to beam diagnostics

Type-II PIGL captures real as well as virtual photons : it acts both as a *near field* and a *far field* detector. Type-II PIGL can therefore be used for beam monitoring, but, like OTR and ODR, it is sensitive to backgrounds from distant radiation sources.

If the particle beam is ultrarelativistic, the quasi-real photons of the Coulomb field at impact parameter up to $b_{\text{max}} \sim \gamma\lambda$ can be captured. They give the

logarithmic increase of (42) with γ and a similar one in (37). They can degrade somewhat the resolution power of Type-II PIGL in transverse beam size measurements, but experience with OTR monitors shows that this effect is not drastic [21, 22, 23, 24].

4 Conclusion

This chapter shows the various possibilities of optical fibers in charged particle beam physics. The phenomenon of light production by a particle passing *near* the fiber, which has some theoretical interest, has not been tested experimentally up to now.

The flexibility of a fiber is an advantage over the delicate optics of OTR and ODR. A narrow fiber has less effects on the beam emittance than the metallic targets used in OTR and ODR.

Much work remains to be done before using the Type-I and Type-II PIGL : find the most convenient wavelength domain (infra-red, visible or ultraviolet) and fiber diameter ; determine the ball-to-fiber transmission coefficients p_f , etc.

The fiber has to be monomode if one wants to emphasize the interference effects. However it would be interesting to make simulations and experiments of the excitations of modes higher than HE_{11} . In particular the $M = 0$ TM mode has a significant E_z component, therefore may be excited at small crossing angle as much as the HE_{11} mode.

References

- [1] X. Artru and C. Ray, Ed. S.B. Dabagov, Proc. SPIE, Vol. 6634 (2007) ; arXiv: hep-ph/0610129.
- [2] X. Artru and C. Ray, Nucl. Inst. Meth. in Phys. Research B **266** (2008) 3725.
- [3] P. Coyle et al, Nucl. Instr. Methods in Phys. Research A **343** (1994) 292.
- [4] A. Contin, R. De Salvo, P. Gorodetzky, J.M. Helleboid, K.F. Johnson, P. Juillot, D. Lazic, M. Lundin, Nucl. Instr. Methods in Phys. Research A **367** (1994) 271.
- [5] E. Janata, Nucl. Inst. Meth. in Phys. Research A **493** (2002) 1.
- [6] H. Henschel, M. Körfer, J. Kuhnenn, U. Weinand and F. Wulf, Nucl. Instr. Methods in Phys. Research A **526** (2004) 537.
- [7] R.J. Glauber and M. Lewenstein, Phys. Rev. A **43**, (1991) 467.
- [8] T. Okoshi, *Optical Fibers*, Academic Press, 1982
- [9] L.S. Bogdankevich, B.M. Bolotovskii, J. Exp. Theoret. Phys. **32**, 1421 [Sov. Phys. JETP **5**, 1157] (1957).

- [10] N.K. Zhevago, V.I. Glebov, Nucl. Instr. Methods A **331** (1993) 592; Zh. Exp. Teor. Fiz. **111** (1997) 466.
- [11] A. Tomita and R. Chiao, Phys. Rev. Lett. **57** (1986) 937.
- [12] J.D. Jackson, *Classical Electrodynamics*, John Wiley & Sons, Inc. (1962).
- [13] W.K.H. Panofsky and M. Phillips, *Classical Electricity and Magnetism*, Addison-Wesley, Inc. (1962).
- [14] T. Kalkbrenner, M. Ramstein, J. Mlynek and V. Sandoghdar, J. Microsc. **202** (2001) 72.
- [15] P. Anger, P. Bharadwaj and L. Novotny, Phys. Rev. Lett. **96** (2006) 113002.
- [16] N. K. Zhevago, Europhys. Lett. **15** (1991) 277.
- [17] F.J. García de Abajo and A. Howie, Phys. Rev. Lett. **80** (1998) 5180.
- [18] N. Yamamoto, K. Araya and F.J. García de Abajo, Phys. Rev. B **64** (2001) 205419.
- [19] G. Naumenko, X. Artru, A. Potylitsyn, Y. Popov, L. Sukhikh and M. Shevelev, J. Phys.: Conf. Ser. **236** (2010) 012004.
- [20] F.J. García de Abajo, Phys. Rev. Lett. **82** (1999) 2776; F.J. García de Abajo, Phys. Rev. E **61** (2000) 5743.
- [21] D.W. Rule and R.B. Fiorito, AIP Conference Proceedings **229** (1991) 315.
- [22] V.A. Lebedev, Nucl. Instr. Methods A **372** (1996) 344.
- [23] J.-C. Denard, P. Piot, K. Capek, E. Feldl, Proc. of the 1997 Particle Accelerator Conference.
- [24] X. Artru, R. Chehab, K. Honkavaara, A. Variola, Nucl. Instr. Methods B **145** (1998) 160.